Supplementary Materials - Ultrafast Transition from State-Blocking Dynamics to Electron Localization in Transition Metal β-Tungsten

E.W. de Vos,* S. Neb, A. Niedermayr, F. Burri, M. Hollm, L. Gallmann, and U. Keller

ELECTRON-ELECTRON THERMALIZATION FITTING PROCEDURE

In order to fit the rise of the ΔOD-features of the few-femtosecond spectrogram (Fig. 2a in the main manuscript), we have followed the example of ref. [1]. We used two separate fits (for the rise associated with the pre- and main-pulse) of a Gaussian error function with a factor of $2\sqrt{\ln(2)}$ in the numerator of the exponent, for direct comparison with the FWHM of the pump-probe temporal cross-correlation:

$$\Delta\mathrm{OD} = c_0 + \frac{c_1}{2}\left[1 + \frac{2}{\sqrt{\pi}}\int_{\infty}^{t} e^{-\left(\frac{2\sqrt{\ln 2}(t'-t_0)}{\tau}\right)^2} dt'\right] \tag{1}$$

Subsequently, we have used Fermi Liquid Theory (FLT) to relate the electron-electron thermalization time (τ_{e-e}) to the final electron temperature T_e. The term 'final electron temperature' refers in this case to the electron temperature directly after electron-electron thermalization has completed, but before the excited carrier population has interacted significantly with the lattice. As mentioned in the main manuscript, the following approximate relation follows from FLT [2, 3]:

$$T_e \approx \frac{1}{k_b \mu_c}\sqrt{\frac{4\hbar E_F}{\pi^3 \tau_{e-e}}} \tag{2}$$

with $\mu_c = r_s/2\pi$ the Coulomb pseudopotential, where $r_s = 3.3$ is the ratio between the Wigner-Seitz radius and the Bohr radius [4]. The values for r_s and $E_F = 5.78$ eV [5] are taken for tungsten rather than β-tungsten because of their availability in literature. The results that we obtain fall within the weak-photoexcitation regime ($k_B T_e \ll E_F$). For tungsten this requirement becomes $T_e \ll 67000$ K, which is easily satisfied.

ESTIMATION OF EXCITED d-STATE POPULATION

In this section we estimate and compare the size of the excited d-state population after optical excitation in previous measurements on titanium [6] and in β-tungsten. We use the PDOS calculation of ref. [7] for titanium and the PDOS calculation from ref. [8] for β-tungsten, which is also depicted in Fig. 1a of the main manuscript. In order to estimate the difference in population between an unexcited ($T_e = 300$ K) and excited distribution, we modulate the DOS of just the d-orbital contributions with the Fermi-Dirac distribution at the calculated final electron temperatures. In the case of β-tungsten this calculation is

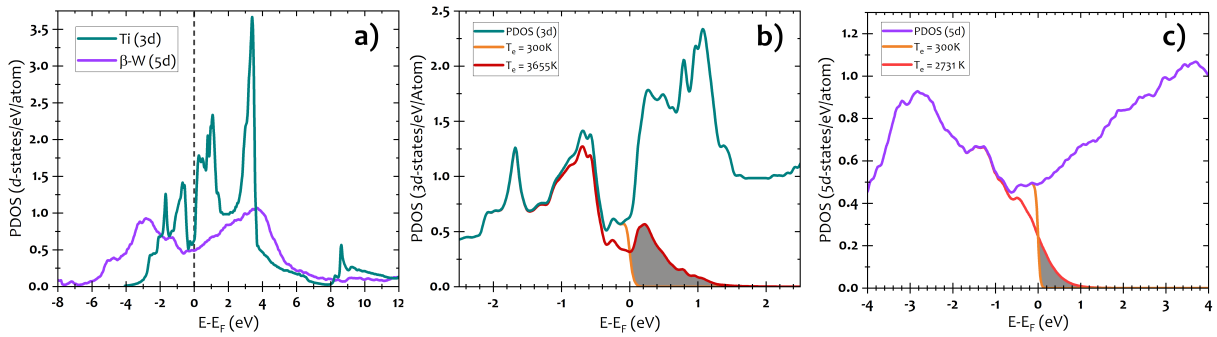

FIG. 1. (a) PDOS calculations of d-orbital contributions for titanium [7] and β-tungsten [8]. (b) PDOS of titanium modulated by the room-temperature Fermi-Dirac distribution (orange) and the excited state Fermi-Dirac distribution (red). The difference between both populations is depicted in dark gray. (c) Same as (b), but for β-tungsten.

discussed in the main manuscript and earlier in the Supplementary Materials. In the case of titanium, we take the excited state temperature of $T_e = 3655$ K $\hat{=}$ 0.315 eV , which was determined via TDDFT calculations in the original publication [6].

The results of this calculation can be seen in Fig. 1. In Fig. 1a the d-orbital contributions to the DOS for both β-W and Ti are depicted. What is immediately noticeable is that titanium exhibits a large concentration of states right above the Fermi level, whereas for β-W the Fermi level lies in the minimum of a pseudo-gap in the DOS. Additionally, the overal magnitude of the d-orbital DOS of titanium is significantly larger around E_F.

Fig. 1b,c depict the change in state-occupation for an increased electron temperature. The occupation at room-temperature is depicted in orange and the occupation at elevated electron-temperature is shown in red. In order to determine the excited state population, we integrate over the difference between these populations (dark gray area). This results in a total excited state density of 0.309 $3d$-states/atom for titanium and 0.077 $5d$-states/atom for β-tungsten.

ACOUSTICAL PHONON & OXIDATION LAYER ANALYSIS

Throughout the spectrogram depicted in Fig. 2, which covers a much longer timescale than the data shown in the main manuscript, two spectrally separated oscillations can be discerned. The most dominant is a long lasting 0.12 THz vibration that is present throughout

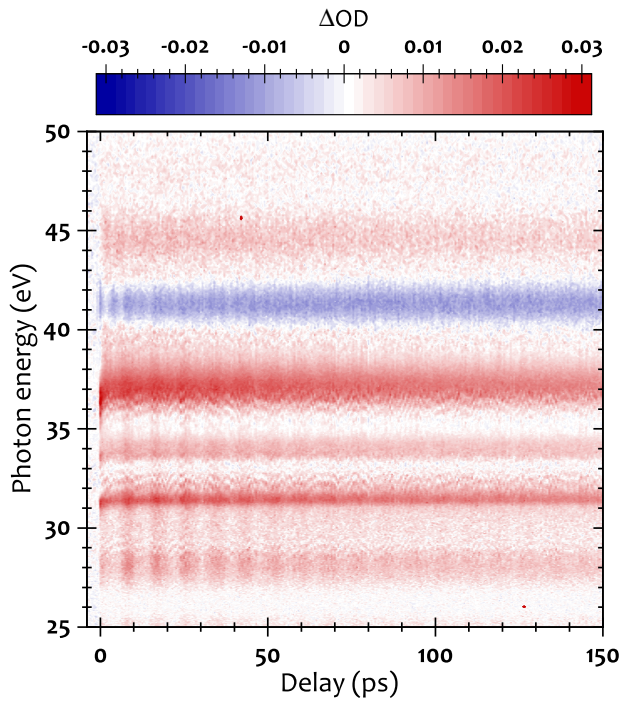

FIG. 2. Transient absorption spectrogram of the picosecond dynamics after pump-probe overlap. Induced opacity is depicted in red and induced transparency in blue. A persistence until t > 150 ps of all features can be observed as well as two spectrally separated oscillations in optical density.

the entire spectrogram. In the region between 40.0 and 42.5 eV, however, an additional phonon is present with a frequency of 0.24 THz that decays within the first 20 ps.

Fig. 3a shows two lineouts of the dynamics after excitation up to a delay of 150 ps. The spectral range of 27.3 - 29.2 eV is chosen to depict the long lasting 0.12 THz vibration and the fast-decaying 0.24 THz oscillation is shown for the region between 40.4 and 42.5 eV. The Fourier spectra of these signals for the selected spectral regions are displayed in Fig. 3b.

The frequencies of the oscillations that are present on the many-ps timescales depicted in Fig. 3a are significantly lower than what is expected for typical optical phonons [9], where the excitation causes a positional vibration of atoms in a unit cell relative to each other. Instead, these frequencies are unique to the sample structure of the material under study deposited onto a thin-film of Si_3N_4 and are most likely indications of the presence of acoustical phonons, also called *blast waves* in literature [10, 11]. The frequency of an acoustical phonon can be approximated to first order by $\nu = v_{\text{long}}/(2L)$, where v_{long} is the longitudinal speed of sound in the propagation medium and L is the thickness along the propagation axis [10, 11]. The

Fourier spectrum that is depicted in Fig. 3b shows a very good agreement between the observed peak of the Fourier spectrum around 0.24 THz and the predicted frequency for a 20-nm thin-film of amorphous Si_3N_4 [13]. The most dominant peak in the Fourier spectrum lies around 0.12 THz and is present throughout the spectrogram. Using the speed of sound for β-tungsten from ref. [14], this peak lies close to the predicted value, 0.102 THz, for an acoustical phonon that travels through a 13.6 nm layer of β-tungsten on top of 20-nm thick Si_3N_4, i.e. one that traverses the entire sample structure. Nevertheless, there is a slight mismatch between the theoretically predicted and the observed value. The same could be said of the shoulder that is present for the spectrum around 0.21 THz and its comparison with the theoretically predicted frequency in just the β-tungsten film. We hypothesise that this mismatch is because of slow thermal evaporation of the thin film of tungsten over the course of many measurements for the areas under excitation. Slight evaporation of the material over time leads to an effectively thinner section of β-W in the area under investigation, which shifts the predicted frequencies to higher values. Working backwards, a 0.12 THz acoustical phonon frequency would amount to a β-W film with an effective thickness of 9.9 nm. The features that are discussed in the main manuscript, however, were not affected by this and were reproducible across 37 measurements over the course of 4 days. Additionally, X-ray diffraction measurements confirmed the sample integrity after the measurements were completed.

In a previous transient absorption study of the semiconductor silicon it was found that the formation of acoustical phonons was mainly dominated by intra-valley electron-phonon scattering and phonon-phonon decay processes [12]. The absence of an optical phonon signature in the transient absorption spectrum of β-tungsten, however, points to a more dominant role of the former process. This is further supported by the fast timescales at which these acoustical phonons are excited.

The black curve in Fig. 3a is a superposition of an exponential decay with a damped sinusoidal oscillation with a frequency of 0.12 THz, fitted to the experimental data:

$$\Delta\mathrm{OD} = A_1 \cdot e^{-t/\tau_1} + A_2 \cdot e^{-t/\tau_2} \cdot \sin\left(\frac{2\pi \cdot (t - t_c)}{T}\right) \tag{3}$$

where $\tau_1 = 443 \pm 25$ ps is the decay constant of the overall decay of the signal, $\tau_2 = 56 \pm 5$ ps is the decay constant of the damped oscillation and $T = 8.60 \pm 0.02$ ps and $t_c = -1.80 \pm 0.08$ ps are the period and phase shift, respectively. The overall decay constant of 443 ± 25 ps

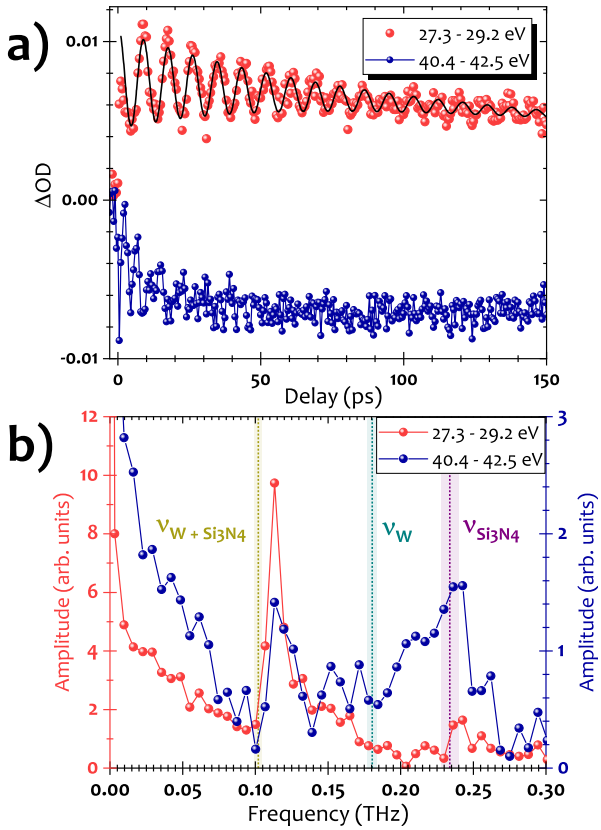

FIG. 3. (a) Lineouts along the temporal axis of the spectrogram depicted in Fig. 4 of the main manuscript, averaged over selected spectral regions. The solid black curve is fitted to the experimental curve as a superposition of a decaying exponential and a damped sinusoidal oscillation. (b) Frequency spectrum of oscillations depicted in (a) compared with theoretical values (vertical dashed lines) and their margin of error (transparent vertical rectangles) for 13.6 nm β-W on top of Si_3N_4. The speed of sound for Si_3N_4 is taken from ref. [13] and the speed of sound for β-W is taken from ref. [14]

shows that this opaque signal decays over hundreds of picoseconds. The magnitude of the signal between 40.4 and 42.5 eV, however, does not decrease significantly within the first 150 ps, indicating a longer lifetime.

The long-lasting nature of this transparent feature stands out both in Fig. 3b of the main manuscript and Fig. 2 of the Supplementary Materials. Two characteristics in particular make it unique within all measurements. The first of these is the fact that it is the only feature that clearly shows the presence of an acoustical phonon that we associate with the propagation of a soundwave within the Si_3N_4 substrate. The second unique characteristic of

this feature is the fact that unlike all other features in the spectrogram, this feature shows no noticeable decay within the first 150 ps. Because there is virtually no background signal for negative delays (i.e. before pump-probe overlap), the signal must decay on nanosecond or microsecond timescales.

Because ATAS measurements are sensitive only to induced changes by the pump pulse and Si_3N_4 is transparent to our NIR excitation spectrum, we do not expect this feature to result from an excitation within the Si_3N_4. However, the sensitivity to an acoustical phonon within Si_3N_4 might stem from the presence of an oxidation layer on the β-W/Si_3N_4 interface. Because the NIR pump is most likely rapidly screened before it penetrates deeper into the β-W, the oxidation layer is probably not directly excited. Rather, the long timescale at which it decays seems to indicate that this signal is mostly thermal in nature and decays through interaction with the environment.

---

* edevos@phys.ethz.ch

[1] H.-T. Chang, A. Guggenmos, S. K. Cushing, Y. Cui, N. U. Din, S. R. Acharya, I. J. Porter, U. Kleineberg, V. Turkowski, T. S. Rahman, D. M. Neumark, and S. R. Leone, Phys. Rev. B **103**, 064305 (2021).

[2] C. Gadermaier, A. S. Alexandrov, V. V. Kabanov, P. Kusar, T. Mertelj, X. Yao, C. Manzoni, D. Brida, G. Cerullo, and D. Mihailovic, Phys. Rev. Lett. **105**, 257001 (2010).

[3] N. W. Ashcroft and Mermin, *Solid State Physics*, 35th ed. (South Melbourne : Brooks/Cole, 2008).

[4] J. H. Rose and H. B. Shore, Phys. Rev. B **48**, 18254 (1993).

[5] M. S. Sodha and P. K. Dubey, J. Phys. D: Appl. Phys. **3**, 139 (1970).

[6] M. Volkov, S. A. Sato, F. Schlaepfer, L. Kasmi, N. Hartmann, M. Lucchini, L. Gallmann, A. Rubio, and U. Keller, Nat. Phys. **15**, 1145 (2019).

[7] E. Bévillon, J. P. Colombier, V. Recoules, and R. Stoian, Phys. Rev. B **89**, 115117 (2014).

[8] A. Chattaraj, S. Joulie, V. Serin, A. Claverie, V. Kumar, and A. Kanjilal, Sci Rep **12**, 3865 (2022).

[9] V. A. Semenov, O. A. Dubovsky, A. V. Orlov, D. V. Savostin, and V. V. Sudarev, Phys. Solid State **56**, 29 (2014).

[10] H. Park, X. Wang, S. Nie, R. Clinite, and J. Cao, Phys. Rev. B **72**, 100301 (2005).

[11] J. Chen, W.-K. Chen, J. Tang, and P. M. Rentzepis, Proceedings of the National Academy of Sciences **108**, 18887 (2011).

[12] S. K. Cushing, M. Zürch, P. M. Kraus, L. M. Carneiro, A. Lee, H.-T. Chang, C. J. Kaplan, and S. R. Leone, Struct. Dyn. **5**, 054302 (2018).

[13] O. A. Lukianova and V. V. Sirota, Ceramics International **43**, 8284 (2017).

[14] A. Nagakubo, H. T. Lee, H. Ogi, T. Moriyama, and T. Ono, Appl. Phys. Lett. **116**, 021901 (2020).